

PREDICTING PERFORMANCE OF ORIENTED STRANDBOARD UNDER CONCENTRATED STATIC LOADING CONDITIONS USING FINITE ELEMENT MODELING

Zheng Chen

Postdoctoral Research Fellow

*Ning Yan**†

Associate Professor

Paul Cooper†

Professor

Faculty of Forestry
University of Toronto
33 Willcocks Street

Toronto, Ontario M5S 3B3
Canada

(Received March 2008)

Abstract. Oriented strandboard (OSB) panels were tested under a concentrated static load (CSL). A finite element (FE) model with variation of stresses and strains in the thickness direction was established to simulate the deflection of OSB under 890-N CSL. The CSL ultimate load of each OSB panel was simulated by increasing the load in the FE model until the calculated stress met the corresponding measured strength. Comparison of the calculated and the experimental data showed that the initial failure had two modes: failure initiated by interlaminar shear stress in the major direction near the central layers and edge of the panel when modulus of rupture (MOR) to interlaminar shear strength ratio in the major direction was greater than 18.8, and failure initiated by bending stress in the major direction near the bottom layers and the loading spot when MOR to interlaminar shear strength ratio in the major direction was less than 17.4. Panel thickness determined the initial failure mode when the ratio of MOR to interlaminar shear strength in the major direction was between 17.4 and 18.8. The vertical density profile affected the distribution of bending stresses and MOR in the profile of panels and influenced the accuracy of the prediction of the FE model.

Keywords: Finite element model, oriented strandboard, concentrated static load, shear stress, bending stress.

INTRODUCTION

Past work has shown that oriented strandboard (OSB) experiences both bending stresses and shear stresses when subjected to a concentrated static load (CSL) (Fig 1). As a result of the complex stresses, the theory for the classic thin orthotropic plate cannot provide a closed-form solution to describe the relationships among stress, strain, force, and deflection of the OSB panels

under concentrated static loading conditions (Timoshenko and Woinowsky-Kriegers 1959; Ashton and Whitney 1970). Therefore, researchers applied numerical methods such as finite element (FE) models to find solutions for those complex problems. Hoyle et al (1982) applied a FE model using thin orthotropic plate theory to study the deflection of composite wood panels under CSL. They compared the FE model-predicted theoretical deflection and the experimentally measured deflection of the OSB panels under CSL applied at the center of the midspan of the panel and at midspan close to one edge of

* Corresponding author: ning.yan@utoronto.ca

† SWST member

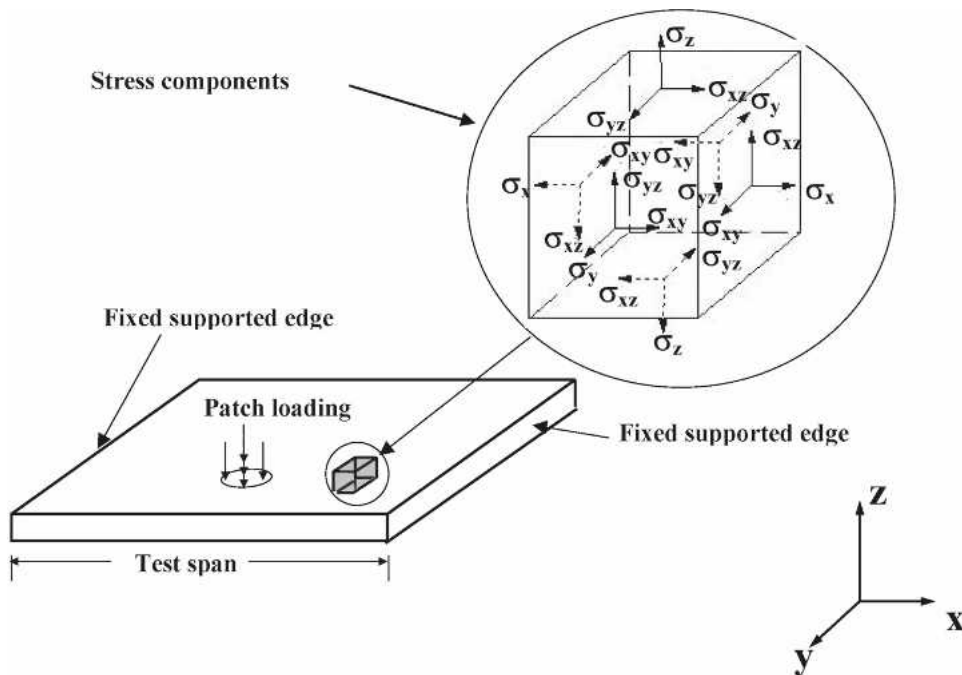


Figure 1. Stress components acting on an element of oriented strandboard panel under concentrated static loading.

the panel. The comparison showed good agreement between the theoretical and experimental results for center-point loading, whereas for edge loading, the agreement was quite poor. The predicted deflection was larger than the experimentally measured values. They attributed the discrepancy to the fact that input parameters to the FE model such as the modulus of rigidity and Poisson's ratios differed from the real panel properties. Xu and Laufenberg (1988) conducted a more detailed theoretical analysis using the Navier-Levy approach for an orthotropic plate supported on two opposite edges that was subjected to a "patch" load. The deflection predicted by their FE model program was less conservative than the prediction by Hoyle et al and agreed better with the experimental results. This improvement was attributed to the fact that the "patch" loading simulated the actual concentrated loading condition better than the "point" loading method used by Hoyle et al in their FE model analysis. This method provided an improved prediction for situations in which the CSL was placed near the free edge of the plate.

However, the applicability of their FE program was limited by an assumed boundary condition of simple support at two edges.

Moarcas and Nicholls (2002) established FE models to determine the "effective width" and "equivalent beam width" in the TRADA calculation method (Soothill 1984) for jointed and unjointed decking subjected to a CSL. Their FE models were based on the thin orthotropic plate theory that included only the bending component. However, it is known that CSL deflection contains both flexural and shear components (Zhang et al 2005; Chen et al 2008). In this regard, Thomas (1996) conducted a parametric study using the FE method to determine the flexural and shear deflections for simply supported and continuous OSB panels. Panels with unsupported edge were not included in his study and he studied only the loading condition with the CSL applied at the center point of the panel. However, the edge loading condition is the standard testing condition in North America and is more demanding for OSB panels. Bozo (2002)

compared the tested CSL properties with the prediction made by a FE model using both average and localized panel density and found that the FE results obtained using the localized density were more accurate.

The objectives of this study were: 1) to establish FE models containing both bending and shear components to simulate the CSL deflection and ultimate CSL of OSB panels according to E661 (ASTM 1997); and 2) to analyze the stress distribution and failure initiation mode by comparing the calculated shear stress and bending stress with the shear strength and bending strength measured by standard tests. The stress and strain variations along the thickness direction of the panels were also considered in this analysis.

FINITE ELEMENT ANALYSIS METHODS

In this study, modulus of elasticity (MOE) and modulus of rupture (MOR) (ASTM 1999), shear strength (ASTM 2000), and deflection under 890-N CSL and ultimate CSL (ASTM 1997) of 15 groups of commercial OSB specimens were measured. The measured MOE and the thickness of the specimens were used as input values for the FE model. MOE in z direction, σ_{xy} , and Poisson's ratios were estimated according to published values (Shresha 1999; Youngquist 1999). The estimated deflection of each OSB panel under 890-N concentrated static load from the FE model was compared with the CSL deflection measured using the standard CSL tests to validate the effectiveness of the model. The ultimate CSL of each panel was simulated by increasing the CSL in the FE model until any type of stress calculated by the FE model reached either the bending or shear strength of that panel. To analyze the influence of panel density on the stress distribution in the panel, the vertical density profile (VDP) of the panels was measured and used as input into the FE model.

FINITE ELEMENT MODEL DEVELOPMENT

The FE model was developed using the commercial FE analysis program (ANSYS INC

2006). To calculate the distribution of the bending stress, interlaminar shear stress, and edge-wise shear stress along the thickness direction of the panel, the 2-D, eight-noded, nonlinear layered quadrangle element (shell 91 in ANSYS program) was used in the FE modeling together with the h -method (Fig 2). Twelve layers of each element were specified according to each panel's thickness. The model dimensions were 406 mm (span of CSL test) \times 610 mm (length of the supported edges in the tested panel). There were 4769 nodes and 1536 elements in one model. Two supported edges in the FE model were considered as fixed edges. In the actual test, CSL was applied to the panel through a 76-mm-dia disk. This was simulated in the FE model by applying loading through a 76-mm-dia circle at the same position as the actual disk. Total load applied through the circle was equal to the CSL specified by the test standard.

To study the influence of VDP on the stress distribution in the thickness direction of the panel, the modulus of each layer in the thickness of the panel is assumed to vary according to its corresponding density. The regression equations between MOE and panel density and MOR and panel density were established according to the standard bending test results. The vertical density profile was measured using an X-ray density profiler. According to the measured VDP, the MOE of each layer of the element was calculated using the obtained regression equations. The stress calculated using the FE model containing varying MOE with the thickness of the panel was compared with the stress obtained from the FE model using the average MOE for the whole panel.

BACKGROUND OF ELEMENT SHELL 91 IN ANSYS PROGRAM

The geometry, node locations, and the coordinate system for this element are shown in Fig 2. The element is defined by eight nodes, layer thicknesses, layer material direction angles, and orthotropic material properties. The stresses and

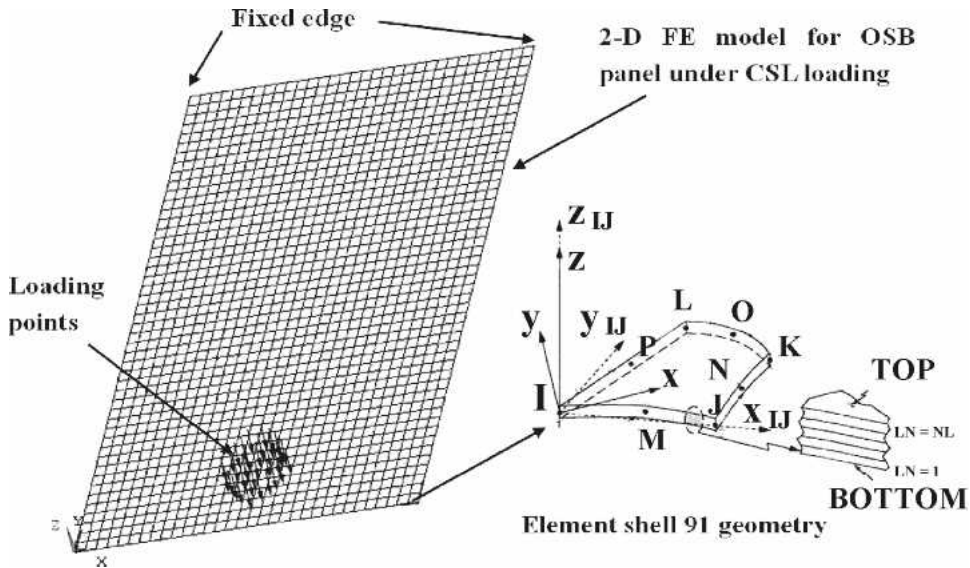


Figure 2. Two-dimensional finite element (FE) model for oriented strandboard under concentrated static loading and its element, shell 91 geometry (ANSYS INC 2006) where, x_{IJ} = element x-axis if element coordinate system number is not supplied. x = element x-axis if element coordinate system number is supplied. LN = layer number. NL = total number of layers. In this study, NL = 12. FE model was automatically meshed. All elements have the same size. Each element size is 12.7×12.7 mm.

strains are variables along the thickness direction.

It is assumed that normal axis to the center plane remains straight after deformation, but not necessarily normal to the center plane. Each triad of integration points (in the r direction) has the same orientation. There is no significant stiffness associated with rotation about the element r axis. The material property matrix, $[D]_j$, for the layer j is:

$$[D]_j = \begin{bmatrix} BE_{x,j} & Bv_{xy,j}E_{x,j} & 0 & 0 & 0 & 0 \\ 0 & 0 & 0 & 0 & 0 & 0 \\ 0 & 0 & 0 & 0 & 0 & 0 \\ 0 & 0 & 0 & G_{xy,j} & 0 & 0 \\ 0 & 0 & 0 & 0 & \frac{G_{yz,j}}{f} & 0 \\ 0 & 0 & 0 & 0 & 0 & \frac{G_{xz,j}}{f} \end{bmatrix} \quad (1)$$

where:

$$B = \frac{E_{y,j}}{E_{y,j} - (v_{xy,j})^2 E_{x,j}} \quad (2)$$

$$f = \left\{ \begin{matrix} 1.2 \\ 1.0 + 0.2 \frac{A}{25t^2} \end{matrix} \right\},$$

whichever is greater.

The in-plane forces are computed as:

$$T_x = \sum_{j=1}^{N_\ell} t_j \left(\frac{\sigma_{x,j}^t + \sigma_{x,j}^b}{2} \right) \quad (3)$$

$$T_y = \sum_{j=1}^{N_\ell} t_j \left(\frac{\sigma_{y,j}^t + \sigma_{y,j}^b}{2} \right) \quad (4)$$

$$T_{xy} = \sum_{j=1}^{N_\ell} t_j \left(\frac{\sigma_{xy,j}^t + \sigma_{xy,j}^b}{2} \right) \quad (5)$$

(1) The out-of-plane moments are computed as:

$$M_x = \frac{1}{6} \sum_{j=1}^{N_\ell} t_j (\sigma_{x,j}^b (2z_j^b + z_j^t) + \sigma_{x,j}^t (2z_j^t + z_j^b)) \quad (6)$$

$$M_y = \frac{1}{6} \sum_{j=1}^{N_\ell} t_j (\sigma_{y,j}^b (2z_j^b + z_j^t) + \sigma_{y,j}^t (2z_j^t + z_j^b)) \quad (7)$$

$$M_{xy} = \frac{1}{6} \sum_{j=1}^{N_\ell} t_j (\sigma_{xy,j}^b (2z_j^b + z_j^t) + \sigma_{xy,j}^t (2z_j^t + z_j^b)) \quad (8)$$

The transverse shear forces are computed as:

$$N_x = \sum_{j=1}^{N_\ell} t_j \sigma_{xz,j} \quad (9)$$

$$N_y = \sum_{j=1}^{N_\ell} t_j \sigma_{yz,j} \quad (10)$$

In this study, the material property matrix, $[D]_j$, was obtained by measurement or by estimation using published data.

MATERIALS AND EXPERIMENTS

The specimens for CSL tests and bending tests were cut from 15 1220- × 2440-mm commercial OSB panels that were manufactured by five companies. Boards A, B, C, and D were from four different companies. Boards HD, LD, MD, and MR were made by the same manufacturer. The panel thicknesses were between 10 and 12 mm. For CSL performance evaluation, 610 × 610 mm specimens were cut from each original panel and tested following E661-88 (ASTM 1997). The test span (support spacing) was 406 mm. CSL deflection was measured under an 890-N load and the ultimate CSL was recorded.

Two 318- × 76-mm specimens from each commercial OSB panel were tested following the D 1037-99 standard bending test (ASTM 1999) to obtain MOE and MOR of the panels. One was cut in the major direction (parallel to surface strand orientation) and one was cut in the minor direction (perpendicular to the surface strand

orientation) of the panels. The test span was 267 mm and loading speed was 5.3 mm/min.

Interlaminar shear strength of the panels was estimated using the D2718-00el (ASTM 2000) standard 5-point test method. The specimens were cut to 356 × 51 mm from the undamaged areas of each panel with one each cut in the major and minor directions. At the loading speed of 1.3 mm/min, the ultimate load was reached within 4–6 min. Only specimens that failed in shear mode were used for the final evaluation of shear effects on the CSL properties. All bending and 5-point tests were done using a Zwick I Z100 test machine (Zwick GmbH & Co, Germany).

The vertical density profile of six specimens from each commercial panel was measured using a QMS QDP-01X Density Profiler (Quintek Measurement Systems Inc, Tennessee).

RESULTS

Simulated Deflection Under an 890-N Concentrated Static Load

The simulated CSL deflection using the FE model vs the experimentally measured CSL deflection are shown in Fig 3. CSL deflections calculated by the FE model were in reasonable agreement with the experimental results. When the influence of VDP on the MOE of the panel layers in thickness was included in the FE model, the agreement improved slightly with the R-square value increased from 0.5 to 0.6. Figure 3 shows that the deflection values estimated by the FE models were lower than the experimental results. Generally, in the FE analysis, the calculated results using the h-method are lower than the actual data (Zienkiewicz and Taylor 2000), and the finer the selected element, the closer the calculated data should be to the actual data. Moreover, in this study, the shear modulus and Poisson's ratio used in the FE model were estimated according to the literature (Shresha 1999; Youngquist 1999) rather than based on measurements of the test material, and that can introduce additional errors.

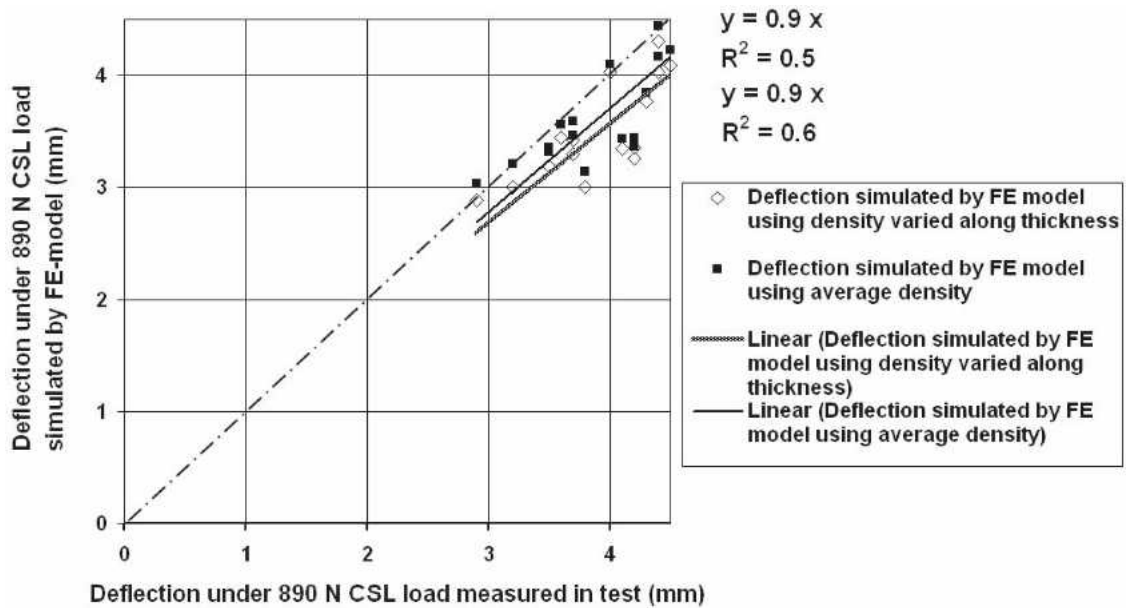


Figure 3. Deflection under 890-N concentrated static load (CSL) simulated by the two finite element (FE) models vs experimental CSL deflection. For FE model, using density varied along thickness of oriented strandboard panels, $y = 0.9x$, $R^2 = 0.6$. For FE models using average density, $y = 0.9x$, $R^2 = 0.5$.

Stress Distribution Profile and Influence of Density

Figures 4–8 show the distribution of the calculated maximum shear stress and bending stress

in the thickness direction of the OSB panel according to the FE model. The distribution profiles for the bending stress and interlaminar shear stress of OSB under CSL are similar in

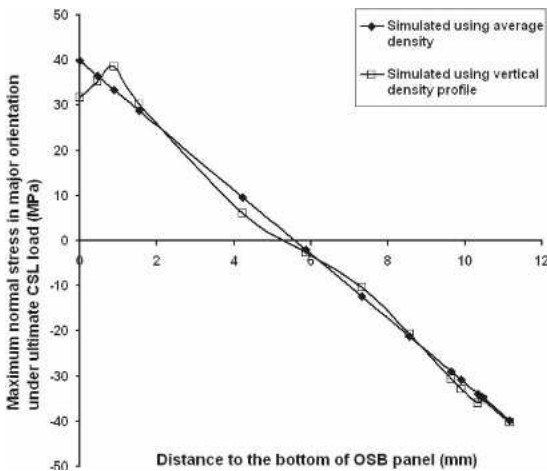


Figure 4. Distributions of the maximum bending stresses in the major direction under the ultimate concentrated static load along the thickness direction simulated by two different finite element models.

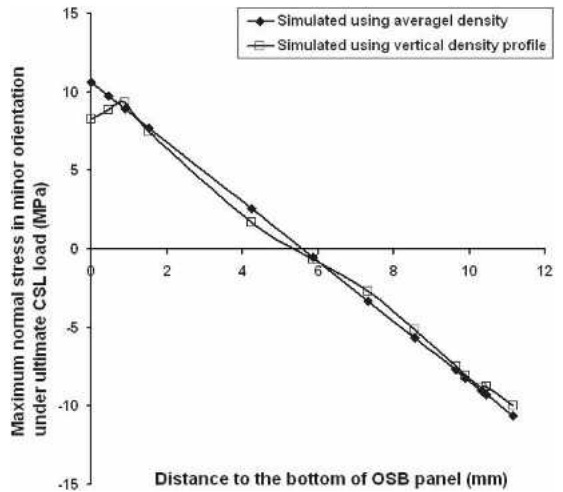


Figure 5. Distributions of the maximum bending stresses in the minor direction under the ultimate concentrated static load in the thickness direction as simulated by two different finite element models.

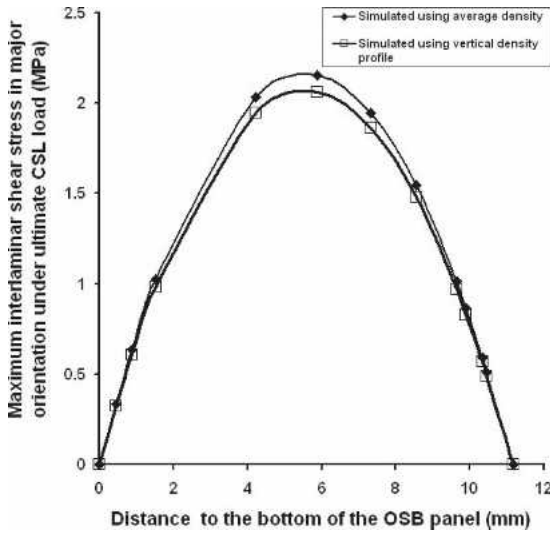


Figure 6. Distributions of the maximum interlaminar shear stresses in the major direction under the ultimate concentrated static load in the thickness direction as simulated by two different finite element models.

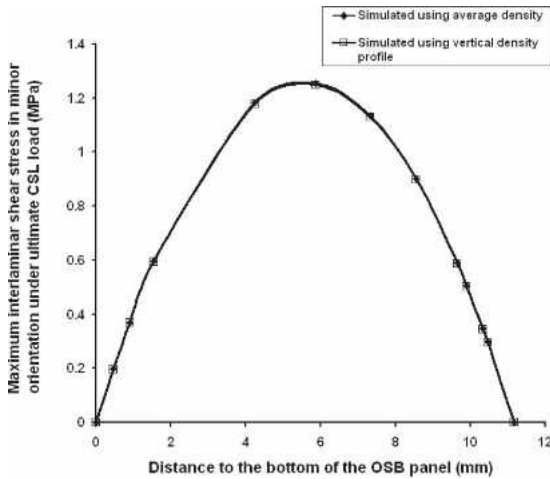


Figure 7. Distributions of the maximum interlaminar shear stresses in the minor direction under the ultimate concentrated static load in the thickness direction as simulated by two different finite element models.

shape to the distribution profiles of the bending stress and shear stress in a rectangular cross-section of a beam under a simple bending load (Bodig and Jayne 1982). The highest maximum bending stress is in the bottom surface and the highest maximum interlaminar shear stress is in

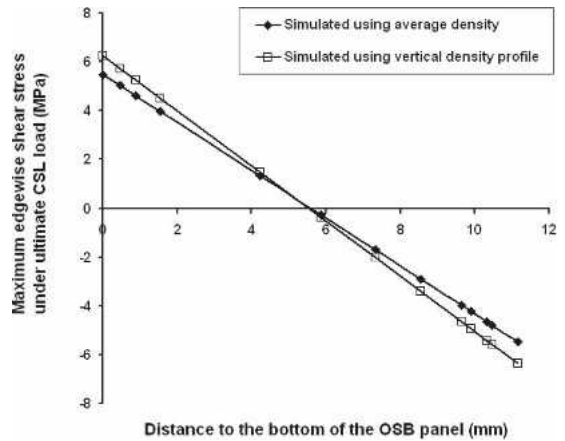


Figure 8. Distributions of the maximum edgewise shear stresses under the ultimate concentrated static load in the thickness direction as simulated by two different finite element models.

the central layer. However, the highest maximum edgewise shear stress lies in the bottom surface of the bottom layer.

The relationship obtained between MOE (MPa) and density (kg/m^3) using the standard bending test results is as follows:

$$E_{xj} = D_j^{1.7951} \times 10^{13} \quad (11)$$

$$R^2 = 0.47$$

$$E_{yj} = D_j^{1.4949} \times 10^{11} \quad (12)$$

$$R^2 = 0.6$$

Using Eqs 11 and 12, the MOE distribution in the thickness direction was estimated using the VDP. Although the difference in structure (such as strand orientation) between a layer within an actual OSB panels and a single-layered panel may influence the relationship between the panel density and MOE for each layer along the thickness direction, we assumed the effect of this discrepancy is minor and evidently some errors could result. The results of the FE model using the MOE profile along the thickness direction indicated that the highest maximum bending stress layer was located near the bottom layer rather than at the bottom layer (Figs 4 and 5). However, the shape of the maximum shear stress

was similar to what was calculated by the FE model using the average MOE.

Based on the bending tests, MOR (MPa) was also found to relate to the panel density (kg/m^3) as follows:

$$\text{MOR}_{xj} = 8D_j^{2.4037} \times 10^{13} \quad (13)$$

$$R^2 = 0.54$$

$$\text{MOR}_{yj} = D_j^{1.5125} \times 10^{13} \quad (14)$$

$$R^2 = 0.68$$

The measured VDP was used in Eqs 13 and 14 to estimate the bending strength (MOR) of the different layers through the thickness of the panel. The results indicated that the highest strength was for the layer near the bottom layer of the element. The comparison of the distributions of MOR and maximum bending stress along the thickness direction is shown in Fig 9. This indicated that the bottom surface of the bottom layer of the panels was still the weakest area, although it was not the location experiencing the highest bending stress in the major direction.

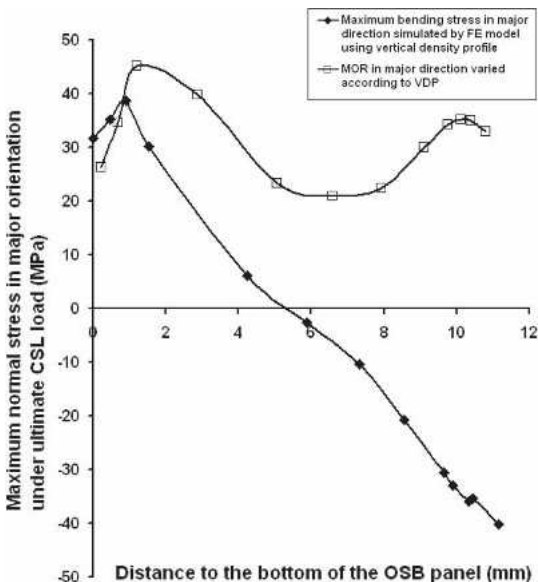


Figure 9. Distribution of the maximum bending stress and modulus of rupture in the major direction along the thickness direction according to the panel vertical density profile.

Finite Element Simulation of Concentrated Static Load Failure Initiation Mode and Ultimate Load

To simulate the failure under CSL of these 15 commercial OSB panels, the MOR measured in the standard bending test was used as the critical value for the bending stress to initiate failure. The critical value of shear stress in-plane was the shear strength measured using the 5-point test. The critical edgewise shear stress was obtained using published data (Shresha 1999; Youngquist 1999). A series of failure initiation stresses were calculated by increasing the CSL step-by-step in the FE model until any type of stress was equal to or larger than its corresponding critical value. The applied CSL corresponding to the stress that initiated failure was considered as the ultimate load simulated by the FE model. Table 1 shows the calculated stress type for each OSB panel that reached the critical value first. It implies that the initial failure was caused either by the bending stress in the major direction exceeding the critical value or by the interlaminar shear stress in the major direction exceeding the critical value.

Table 1 also lists the ratio of MOR to interlaminar shear strength in the major direction and the corresponding thickness value for each commercial panel. It indicates that the failure was initiated as a result of the interlaminar shear stress in the major direction when the ratio of MOR to interlaminar shear strength in the major direction was equal to or greater than 18.8. The failure was initiated by the bending stress in the major direction when the ratio of MOR to interlaminar shear strength in the major direction was equal to or less than 17.4. The failure initiation mode depended on the panel thickness if the ratio of MOR to interlaminar shear strength in the major direction was between 17.4 and 18.8. In this range, failure in the thinner panels was initiated largely by the bending stress in the major direction, whereas the failure in the thicker panel originated primarily from the interlaminar shear stress in the major direction.

When the failure was caused by the bending stress in the major direction, the failure spot was

Table 1. Failure initiation mode and location of the initial failure under the CSL ultimate load simulated by the FE model and the corresponding ratio of MOR to interlaminar shear strength in the major direction and thickness of the panels.

Panel no.	The predicted stress responsible for failure initiation	Failure location (x axis (mm) Figure 2)	Failure location (y axis (mm) Figure 2)	Ratio of MOR to interlaminar shear strength (major direction)	Thickness (mm)
D1	Bending in major direction	203.2	38.1	14.2	11.44
D2	Bending in major direction	203.2	38.1	15.7	11.16
C2	Bending in major direction	203.2	38.1	16.1	10.7
A1	Bending in major direction	203.2	38.1	17.0	11.15
C1	Bending in major direction	76.2 and 330.2	38.1	17.4	11.11
A2	Bending in major direction	203.2	38.1	18.5	10.81
LD1	Interlaminar shear in major direction	76.2 and 330.2	0	18.3	11.01
LD2	Interlaminar shear in major direction	76.2 and 330.2	0	18.8	11.21
B1	Interlaminar shear in major direction	76.2 and 330.2	0	19.4	11.21
MD2	Interlaminar shear in major direction	76.2 and 330.2	0	22.7	11.29
HD1	Interlaminar shear in major direction	76.2 and 330.2	0	20.3	11.31
B2	Interlaminar shear in major direction	76.2 and 330.2	0	19.6	11.32
MR1	Interlaminar shear in major direction	76.2 and 330.2	0	21.1	11.37
MD1	Interlaminar shear in major direction	76.2 and 330.2	0	19.1	11.73
HD2	Interlaminar shear in major direction	76.2 and 330.2	0	20.8	11.84

found to be inside the loading disk area at the bottom of the panel (Fig 10). When the initial failure was produced by the interlaminar shear stress in the major direction, the failure spot was

located within the center layer of the panel close to the unsupported edge near the disk (Fig 11). The actual failure point depended on the location of the weak spot within the panel and the accu-

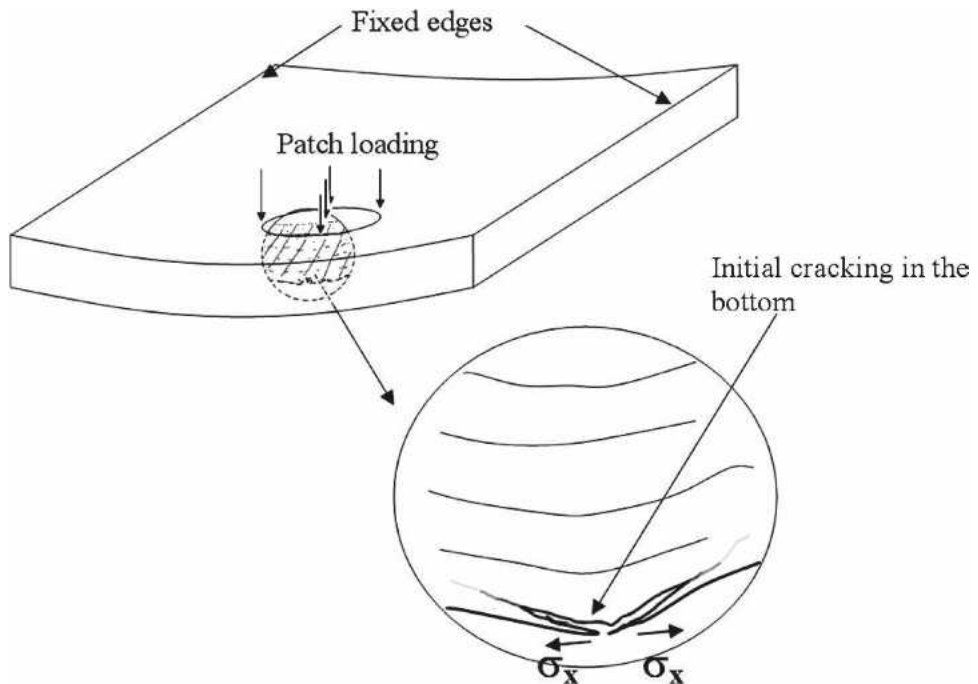


Figure 10. Initial failure produced by the bending stress in the major direction under the concentrated static ultimate load.

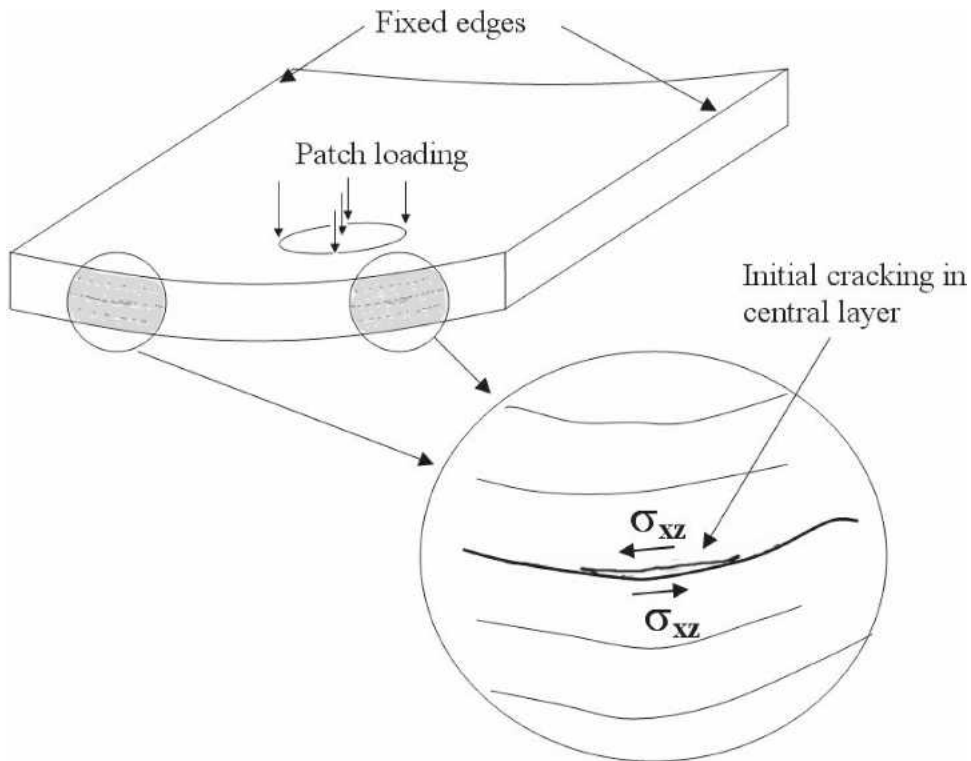


Figure 11. Initial failure produced by the interlaminar shear stress in the major direction under the concentrated static ultimate load.

curacy of the center positioning of the loading disk between the two supported edges. Figures 12 and 13 show the distribution contour plots of the bending stress and interlaminar shear stress in the major direction in the panel under the ultimate CSL.

Comparison of the simulated ultimate CSL with the experimental measured ultimate CSL (Fig 14) showed that all calculated values were lower than the experimental results. The estimation by the FE model is more conservative. However, the slope and the R-square value of the calculated data using the FE model vs the experimental data of the ultimate CSL were 1.0 and 0.7, respectively. It indicates that the prediction of the trend for the ultimate CSL by the FE model is reasonable.

DISCUSSION

In this study, FE models were developed that included both the bending and shear compo-

nents. The model, after incorporating the shear component, gave a better prediction of the CSL deflection than some other FE models previously reported in the literature that did not consider the shear component (Hoyle et al 1982; Xu and Laufenberg 1988). The FE model used in this study also took into consideration the stress and strain variations in the thickness direction. Comparing the model predictions of this study with that of a FE model in a previous study that did not consider the variation in stress and strain in the thickness direction (Bozo 2002), the R-square value and the slope of the regression line of the model predictions vs experimental measurements for the CSL deflection are higher in this study (slope of the regression line = 0.9, $R^2 = 0.5$ vs slope of the regression line = 0.6, $R^2 = 0.47$). Therefore, incorporating the variation of the stress and strain in the thickness direction of the panel improved the prediction. Thomas (1996, 2002) also neglected the varia-

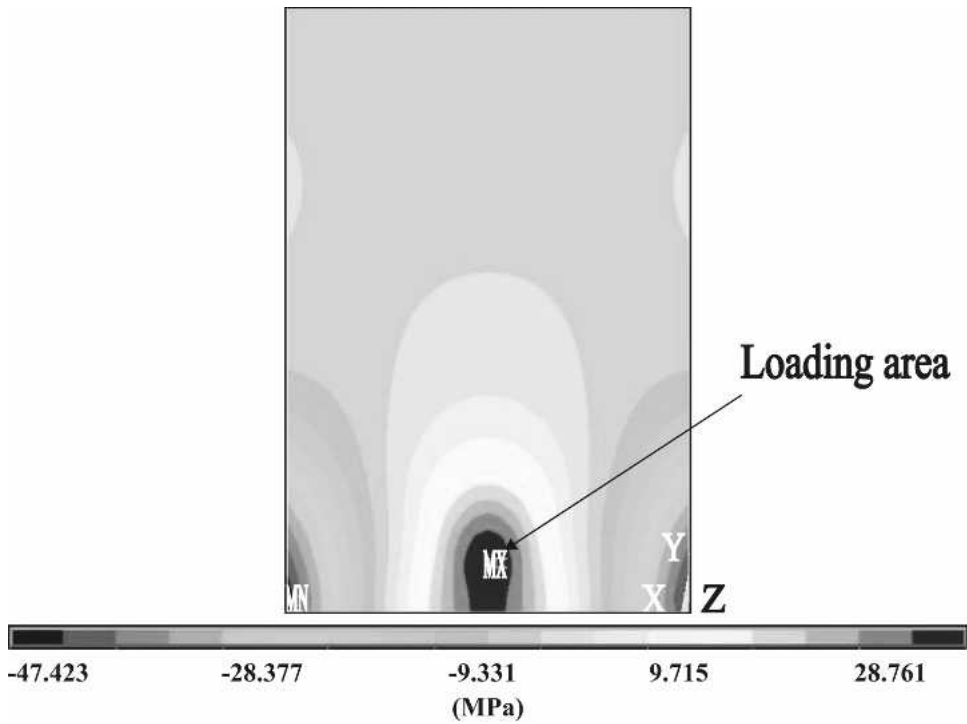


Figure 12. Distribution of the bending stress in the major direction in the bottom of the bottom layer under the ultimate concentrated static load as simulated by the finite element model.

tion of the stress and strain along the thickness direction when he used his FE model to calculate the bending deflection and shear deflection of the OSB flooring deck under a centrally located point load. The FE model that Thomas used to calculate the total deflection (both shear deflection and bending deflection) under a centrally located CSL included shear deflection. However, he assumed that the transverse shear stresses (σ_{xz} and σ_{yz}) were constant through the thickness of the panel. It is well known that OSB panels typically consist of different layers and can vary widely in properties through the thickness. Thus, if the stress and strain variations in the thickness of the panel were included in the Thomas model, the model predictions would perhaps have been more accurate.

Although the predicted bending stress distribution in the thickness direction was influenced by the VDP of the panel, it did not change the fact that the bottom of the panel, as the weakest area,

initiated the bending failure. A more realistic prediction of the bending stress and strain distribution could help to better describe the failure propagation in the thickness direction of the panel. The key influence of the ratio of MOR to interlaminar shear strength in the major direction on the failure initiation mode could provide the OSB manufacturers with better insight into how to improve the CSL performance of their OSB panels.

CONCLUSIONS

An FE model that takes into account the variations of the stress and strain in the thickness direction was developed to describe the CSL performance of the OSB panels. Compared with experimental results, the model gave reasonable predictions of the CSL deflection and ultimate CSL. Although the predictions of the FE model were still more conservative than the actual CSL

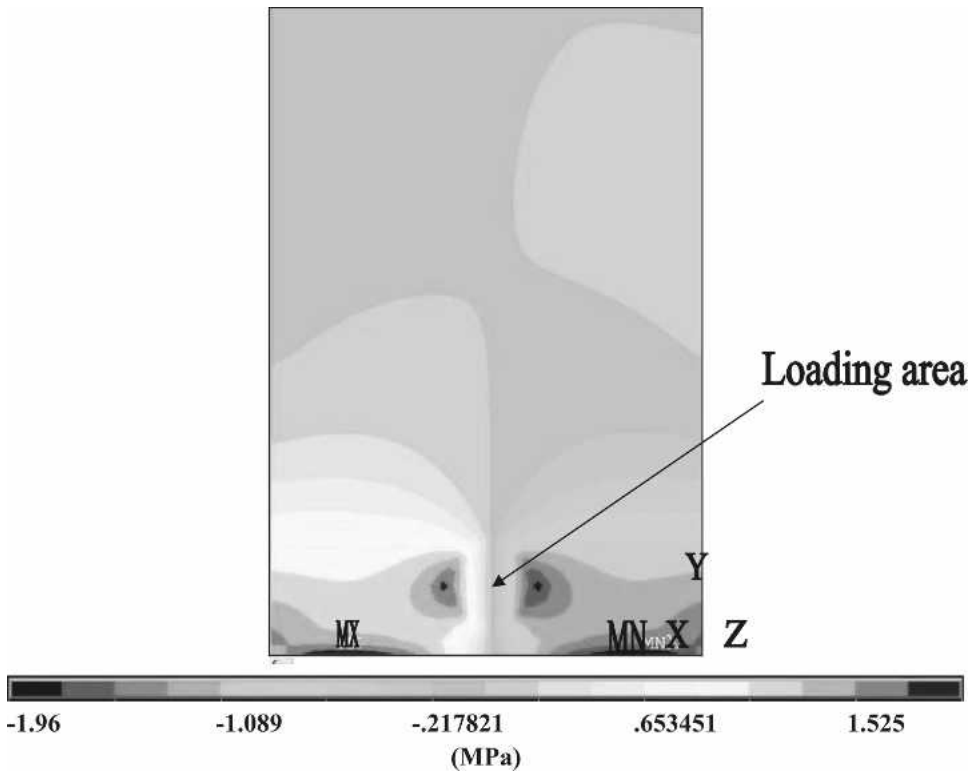


Figure 13. Distribution of the interlaminar shear stress in the major direction in the central layer under the concentrated static ultimate load as simulated by the finite element model.

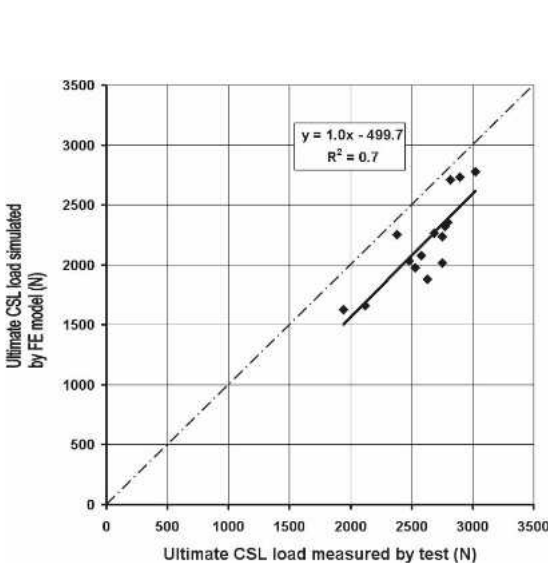


Figure 14. Ultimate concentrated static load (CSL) simulated by the finite element model vs the experimentally measured ultimate CSL.

data, the results of this FE model were slightly more accurate than those of the previously developed FE models that assumed stress and strain were constant along the thickness direction.

The influence of VDP changed the distribution of the bending stress in both major and minor directions along the thickness of the panel. However, it did not change the distribution of the shear stress in the thickness direction.

According to the FE model, failure of the panels used in this study was initiated only by the bending stress in the major direction or by the interlaminar shear stress in the major direction. The initial failure mode depended on the ratio of MOR to the interlaminar shear strength of the panel in the major direction and the thickness of the panel. In this study, interlaminar shear stress resulted in the initial failure when the ratio of MOR to interlaminar shear strength was greater

than or equal to 18.8, whereas the bending stress caused the initial failure when the ratio of MOR to interlaminar shear was less than or equal to 17.4. With a ratio of MOR to interlaminar shear strength between 17.4 and 18.8, the thinner panels failed under the bending stress in the major direction and the thicker panel failed under the interlaminar shear stress in the minor direction.

The weakest spot in the OSB panel under a CSL (ASTM 1997) was located in the loading disk area at the bottom of the panel when the initial failure was caused by the bending stress. When the interlaminar shear stress was the cause for the failure initiation, the weakest spot was located within the center layer of the panel between the loading disk area and the closest unsupported edge.

LIST OF NOTATIONS

- x = major direction, aligned with the test span direction and surface strand orientation of the OSB panel
 y = minor direction, perpendicular to the test span and surface strand orientation of the OSB panel
 z = thickness direction of the OSB panel; z coordinate is normal to the basic units of finite element structural system: two-dimensional elements shell in finite element structural system, with $z = 0$ at the shell mid-surface
 σ_x = bending stress in major direction
 σ_y = bending stress in minor direction
 σ_z = bending stress in thickness direction
 σ_{xz} = interlaminar shear stress in major direction
 σ_{yz} = interlaminar shear stress in minor direction
 σ_{xy} = edgewise shear stress
 D_j = density in layer j of the panel
 E_x = modulus of elasticity in major direction
 E_y = modulus of elasticity in minor direction
 $E_{x,j}$ = modulus of elasticity in major direction of layer j

- $E_{y,j}$ = modulus of elasticity in minor direction of layer j
 $MOR_{x,j}$ = modulus of rupture in major direction of layer j
 $MOR_{y,j}$ = modulus of rupture in minor direction of layer j
 $\nu_{xy,j}$ = Poisson's ratio in x-y plane of layer j
 $G_{xy,j}$ = shear modulus in x-y plane of layer j
 A = element area (in s-t plane)
 t = average total thickness
 T_x = in-plane x force per unit length
 N_ℓ = numbers of layers
 $\sigma_{x,j}^t$ = bending stress at top of layer j in element major direction
 $\sigma_{x,j}^b$ = stress at bottom of layer j in element major direction
 t_j = thickness of layer j
 M_x = x-moment per unit length
 z_j^b = coordinate of bottom layer j
 z_j^t = coordinate of top layer j
 N_x = transverse x-shear force per unit length
 $\sigma_{xz,j}$ = average interlaminar shear stress in layer j in element x-z plane

REFERENCES

- ANSYS INC (2006) ANSYS, Version 10.0. Canonsburg, PA.
 Ashton JE, Whitney JM (1970) Theory of laminated plates. TECHNOMIC Publishing Co Inc, Westport, CT.
 ASTM (1997) Standard test method for performance of wood and wood-based floor and roof sheathing under concentrated static and impact loads. E661-88. American Society for Testing and Materials, West Conshohocken, PA.
 ——— (1999) Standard test methods for evaluating properties of wood-base fiber and particle panel materials. D1037-99. American Society for Testing and Materials, West Conshohocken, PA.
 ——— (2000) Standard test methods for structural panels in planar shear (rolling shear). D2718-00el. American Society for Testing and Materials, West Conshohocken, PA.
 Bodig J, Jayne BA (1982) Mechanics of wood and wood composites. Van Nostrand Reinhold Company Inc., New York, NY.
 Bozo AM (2002) Spatial variation of wood composite. PhD Thesis. Washington State University, Pullman, WA.
 Chen Z, Yan N, Cooper P (2008) Effect of panel properties on the concentrated static load (CSL) performance of

- oriented strand board (OSB). *Holz Roh Werkst* 66(3): 207–212.
- Hoyle RJ, Tichy RJ, Itani RY (1982) Composite wood panel deflection under concentrated load. *Wood Sci* 15(2):65–77.
- Moarcas O, Nicholls T (2002) Concentrated loads on floor deckings. Part 2: Design recommendations. *J Inst Wood Sci* 16(2):93–103.
- Shresha D (1999) Shear properties tests of oriented strand-board panels. *Forest Prod J* 49(10):41–46.
- Soothill C (1984) Concentrated load capacity (punching shear strength) of wood chipboard. Part 2: Assessment of the influence of bending on the resistance of flooring chipboard to gradually applied concentrated loads. Research Report 2/84. Timber Research & Development Association (TRADA), Hughenden Valley, UK.
- Thomas WH (1996) Bending behavior of OSB decking under concentrated load. PhD Thesis. Department of Civil Engineering, University of Surrey, Guildford, Surrey, UK.
- (2002) Shear & flexural deflection equations for OSB floor decking with point load. *Holz Roh Werkst* 60:175–180.
- Timoshenko S, Woinowsky-Kriegers S (1959) *Theory of plate and shells*. 2nd ed. McGraw-Hill, New York, NY.
- Xu D, Laufenberg TL (1988) Orthotropic plate deflection under concentrated load. Research Paper FPL-RP. USDA Forest Service, Forest Products Laboratory, Madison, WI.
- Youngquist JA (1999) Wood-based composites and panel products. *Wood handbook—Wood as an engineering material*. USDA Forest Service, Forest Products Laboratory, Madison, WI.
- Zhang Y, Yan N, Cooper PA (2005) The relationship between concentrated static load performance and other physical and mechanical properties of OSB panels. *Forest Prod J* 55(12):148–152.
- Zienkiewicz OC, Taylor RL (2000) *Finite element method*. 5th ed. Vol. 1. The basis. Butterworth-Heinemann, Oxford, UK.